

Beam tests for the determination of the interfacial properties of FRCM composites

Maria Teresa Cristofaro^{a,*}, Angelo D'Ambrisi^a, Francesco Focacci^b,
Marco Tanganelli^a, Mario De Stefano^a

^a Dipartimento di Architettura, Università di Firenze, piazza Brunelleschi 6, 50121 Firenze, Italy

^b Università eCampus, via Isimbardi 10, 22060 Novedrate, CO, Italy

ARTICLE INFO

Keywords:

FRCM composites
RC structures
Experimental campaign
Beam test
Cohesive material law

ABSTRACT

Fiber Reinforced Cementitious Matrix (FRCM) materials are widely used for strengthening reinforced concrete (RC) structures. Experimental studies show that the collapse of RC elements reinforced with FRCM composites occurs due to the loss of bond of the reinforcing material. For this reason the issue of the shear stress transfer between reinforcement and concrete substrate has been extensively studied in the last years. The single-lap shear test is the most frequently adopted test configuration. In this paper the results of bond tests between a FRCM composite and concrete performed in the beam test configuration are presented. The results are used to determine the cohesive material law (CML) of the tested composite and the obtained CML is compared with that obtained on the basis of the results of single-lap shear tests. The comparison shows that the two test configurations provide similar CML.

1. Introduction

Fiber reinforced polymers (FRP) [1,2] and fiber reinforced cementitious matrix (FRCM) composites [3,4] are widely used for strengthening and repairing masonry and reinforced concrete (RC) structures. The former are made of continuous fibers embedded in a polymeric matrix, whereas the latter consist of continuous fibers arranged in unidirectional or bidirectional textiles embedded in a cement based matrix. FRCM composites proved to be effective in increasing the flexural [5–10] and the shear [11–13] capacity of RC members.

Guidelines have recently been issued for the mechanical characterization and evaluation of the design parameters of FRCM composites [14,15]. Italian guideline [14] provides for tensile tests both on textiles and on composites and direct shear tests, whereas US guideline [15] provides for tensile tests on composites and tests on structural elements.

The effectiveness of composite materials in increasing the flexural and shear capacity of concrete and masonry structural elements strongly depend on the bond properties between composite and substrate (FRP) [1,16,17] and between fibers and matrix (FRCM) [18, 19]. Conversely, in the case of confinement of concrete and masonry columns the effectiveness of the composite material does not require shear stress transfer at the reinforcement-substrate interface [20], since the confining action is produced by the lateral expansion of the structural element associated with the axial force. In the case of confinement, bond shear stresses are required at the fiber-matrix interface in the overlapped length only, to guarantee the presence of tensile stress in the fibers.

* Corresponding author.

E-mail address: mariateresa.cristofaro@unifi.it (M.T. Cristofaro).

The shear stress transfer at the reinforcement-substrate interface is experimentally studied through direct shear tests in the single-lap configuration [21–27] (Fig. 1a) or double-lap [23,28] configuration (Fig. 1b). These tests are performed to determine the debonding mechanism, i.e., the interface where debonding occurs, the maximum force transferable at the interface, named joint capacity, the maximum force transferable when debonding initiates, named debonding load [13,27], and the minimum length of the interface surface to obtain the bond capacity, named effective bond length. The tests performed so far have shown that for many FRCM materials the debonding occurs at the interface between fiber and matrix with significant relative displacements of the fibers with respect to the matrix and without debonding of the matrix from the support [29,30].

The results of the single-lap or double-lap shear tests can be used to obtain a cohesive material law (CML) [25,27,31], i.e., a relationship between the interfacial shear stress τ and the relative displacement or slip s between the fibers and the substrate. In the case of FRCM materials that show a loss of bond at the interface between fibers and matrix, the CML allows to predict with reasonable accuracy the tensile response obtained through tensile tests [32–35] performed according to AC 434 [15].

An alternative to direct shear tests for the evaluation of the interfacial properties is the indirect shear test performed on specimens of the beam test type [36–39] (Fig. 1c). The beams are made up of two concrete blocks connected by a hinge in the compression zone and by the reinforcement in the tensile zone and are subjected to bending test on 3 or 4 load points. The maximum tensile force N in the composite material (i.e., the force at the hinged cross-section) is determined as a function of the applied force F through equilibrium conditions.

In this work, the results of an experimental campaign of beam tests on two FRCM composites with PBO (poliparafenilenbenzobisoxazole) fibers (PBO-FRCM) are presented. The PBO-FRCM considered are characterized by different PBO textiles embedded in the same cement based matrix. Many experimental results can be found in literature on the bond properties of FRCM composites [13]. In particular, the results of single-lap shear tests performed with different bond lengths are reported in [26]. In [27] the results presented in [26] are used to calibrate an interfacial CML based on the relationship between bond length and joint capacity, named joint capacity response. In [23,38] the results of single-lap shear tests are compared with the results of double-lap shear tests. In [40] the dependence of the joint capacity evaluated with single-lap shear test on the loading rate is highlighted. Finally in [38] beam test results are compared with single-lap shear test results and it is observed that these two tests provide comparable results in terms of debonding load and joint capacity.

The experimental campaign presented in this paper includes beam tests on PBO-FRCM materials characterized by two PBO textiles. The tests were performed at different loading rates. The obtained experimental results are discussed and compared with the experimental results available in literature with the following aims: i) to compare the dependence of the joint capacity on the loading rate obtained with single-lap shear tests with the dependence of the joint capacity on the loading rate obtained with the beam test; ii) to assess the influence of the fiber arrangement in textiles on the fiber stress associated with the joint capacity; iii) to compare the results of single-lap shear tests with the results of beam tests in terms of joint capacity. Finally, the procedure proposed in [41] is used to determine the CMLs of the tested FRCM composites based on the results of beam tests. For one of the tested FRCM composite, the obtained CML is compared with: i) the CML obtained for the same FRCM composite by Focacci et al. [27] based on the results of single-lap shear tests using an indirect calibration method based on the joint capacity response, and ii) the CML obtained for the same FRCM composite by D'Antino et al. [26] using a direct calibration method based on the profile of the strain along the bonded length. The main novelties presented in the paper are as follows: i) use of beam test to assess the dependence of the joint capacity on the loading rate and to compare the bond performances of two different textiles embedded in the same cement-based matrix; ii) use of beam test to obtain the load responses of PBO-FRCM composites and comparison of these load responses with those obtained by means of single-lap shear tests; iii) extensive application of the simple procedure proposed in [41] to obtain the CML of the tested PBO-FRCM composites and comparison with the CMLs obtained with more complex procedures.

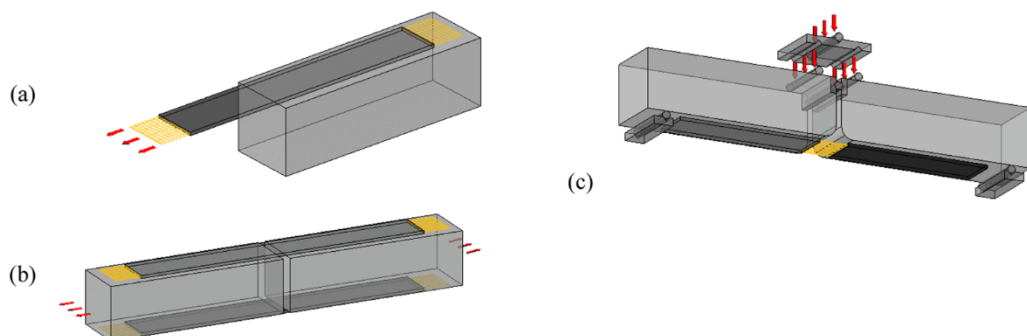


Fig. 1. Typical test setup for (a) single-lap shear test, (b) double-lap shear test, and (c) beam test.

2. Experimental program

2.1. Materials

Two different PBO textiles (Fig. 2) embedded in the same cement matrix were used in the experimental campaign: i) bidirectional textile with 70 g/m² of fiber in the longitudinal direction (equivalent thickness of 0.046 mm) and 18 g/m² of fibers in the transversal direction (equivalent thickness of 0.012 mm); ii) unidirectional textile with 105 g/m² of fibers (equivalent thickness of 0.067 mm).

These PBO textiles are referred to as 70/18, and 105, respectively. The main geometrical and mechanical properties of the PBO textiles are summarized in Table 1, where b^* , t^* and l_f are the width, thickness and center-to-center distance of the longitudinal yarns, respectively, while t_f is the equivalent thickness, defined as the cross section area per unit width, equal to $t^*b^*/l_f = p/\gamma_f$, where $p = 70$, or 105 g/m² is the weight of the longitudinal fibers per unit surface of the textile and $\gamma_f = 1.56$ g/cm³ is the unit weight of the PBO fibers. E_f is the elastic modulus of the PBO fiber assumed equal to 206 GPa according to the tensile tests presented in [26], and f_t is the fiber tensile strength according to the manufacturer.

The cement based matrix was characterized through three-point bending tests and compression tests [42]. The performed tests provided an average compressive strength of 29.13 MPa and an average tensile strength of 6.40 MPa. The concrete blocks were casted with a commercial mix design (C25/30 concrete produced by BigMat [43]) with the addition of 20 % river sand (grain size of 0.3 ÷ 1.25 mm) to obtain strength values close to those typical of existing RC buildings. Simultaneously to the block casting, 20 cubes with a side of 150 mm were casted. The compression tests of these cubes, performed according to [44], provided an average compressive strength of 17 MPa (CoV 11 %).

2.2. Test setup

The bonded length L was the same for the two blocks and was equal to 363 mm. The width of the strip b_c was equal to 94 mm (Fig. 3). 10 and 9 PBO yarns are arranged in the width b_c for the 70/18 and 105 textile, respectively.

The bond length L was greater than the effective bond length L_{eff} which is approximately 250–280 mm according to [26,27,31]. This allowed to reach the debonding load of the reinforcement and therefore to compare the obtained results with those of single-lap shear tests with $L \geq L_{eff}$ in terms of debonding load. The edges of the concrete blocks were rounded at the intrados of the hinged cross sections to reduce the transverse compressive stresses at the interface associated with the relative rotation between the blocks during the test [13,37].

The tests were performed with a servo-hydraulic universal testing machine (Instron) by controlling the stroke of the machine a constant rate. During the test the following response parameters were measured: i) the applied force F (Fig. 3a); ii) the relative displacement δ between the blocks at the intrados (evaluated as the average measure of transducers T1 and T2 in Fig. 3a); iii) the slips g_R and g_L of the fibers at mid-span with respect to the two blocks (measured by transducers T4 and T5, respectively). In particular, g_R and g_L (transducers T4 and T5) are the maximum relative displacements between the fibers and the concrete blocks (slips at points A and A'), which are referred to as global slips of the interface surfaces. The T1 and T2 transducers were of the CDP (LVDT) type with movable shaft, while the T4 and T5 transducers were of the CE cantilever type. Four displacement rates were used for the stroke of the machine: 0.17, 0.34, 0.51 and 0.68 mm/min.

Samples were named $BT_{x_yf_zn}$, where x indicates the type of textile (70/18 or 105), y the number of yarns, z the displacement rate, and n the number of the sample. The samples are listed in Table 2. At least three nominally equal specimens were tested for each textile and for each rate. Pictures of representative test samples are shown in Fig. 4.

The adopted displacement rates correspond to nominal slip rates of 0.00085, 0.0017, 0.00255 and 0.0034 mm/s, respectively. The elastic deformation of the concrete blocks was neglected when computing the nominal slip rate associated with each displacement rate

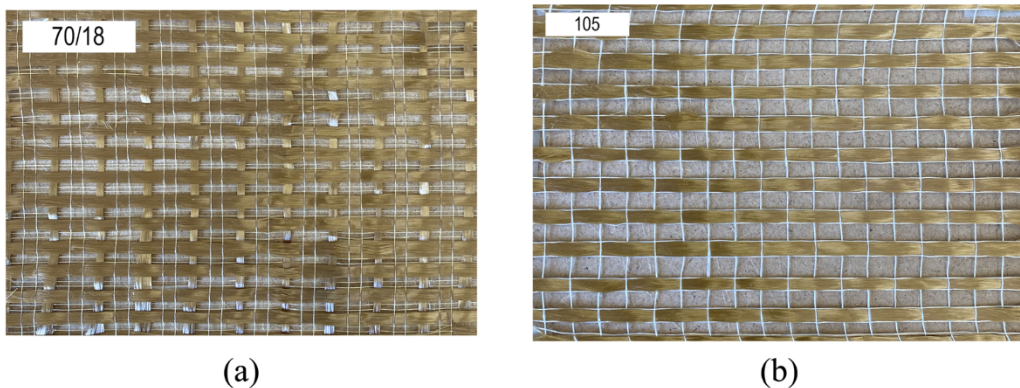
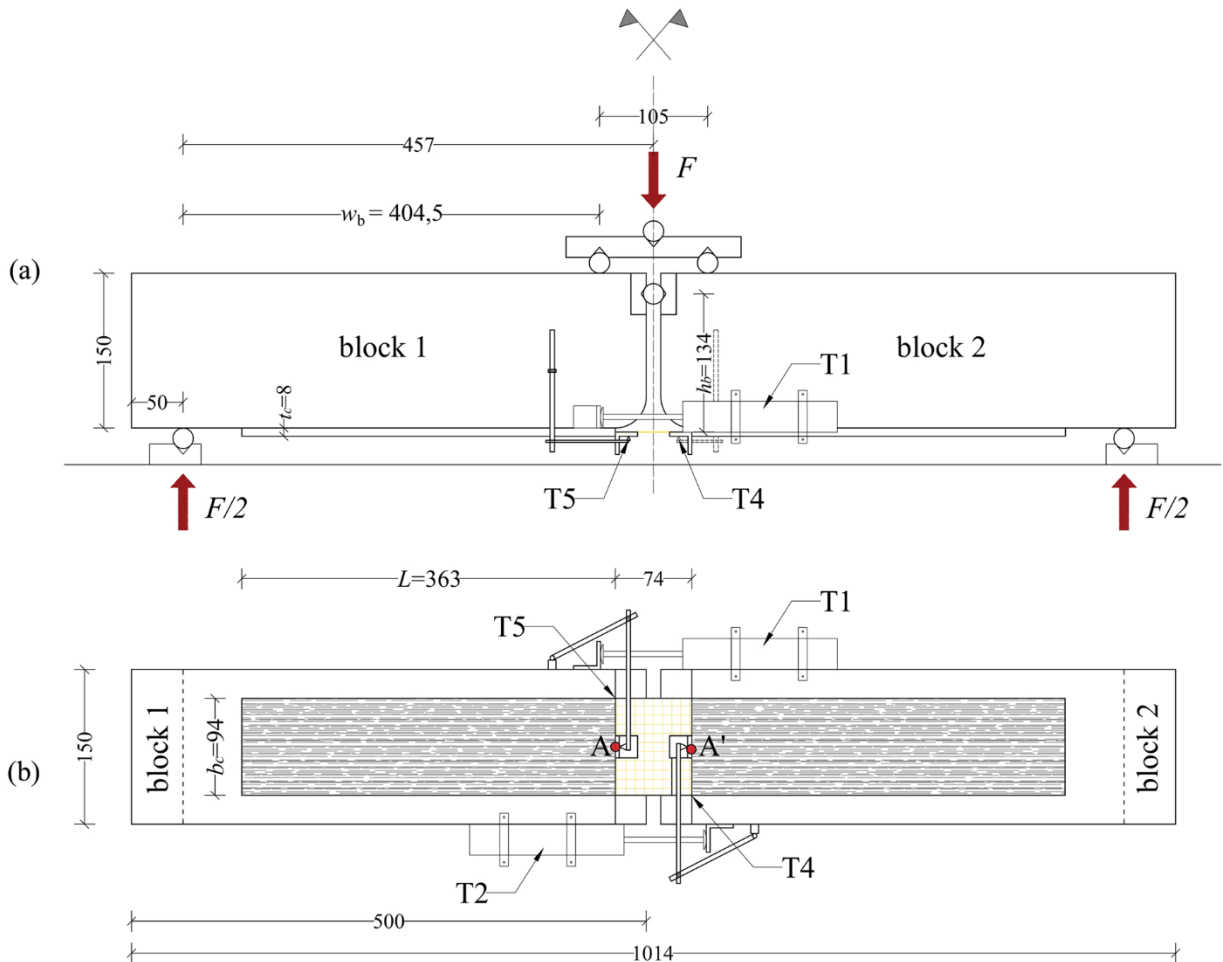


Fig. 2. PBO textiles used in the tested FRCC materials: (a) bidirectional textile with 70 g/m² of fibers in the longitudinal direction and 18 g/m² of fibers in the transversal direction; (b) unidirectional textiles with 105 g/m² of fibers in the longitudinal direction.

Table 1

Geometrical and mechanical properties of the two different PBO textiles.

PBO textile	p [g/m ²]	b^* [mm]	t^* [mm]	i_f [mm]	t_f [mm]	E_f [GPa]	f_t [GPa]
70/18	70	4	0.1081	9.5	0.046	206	5.8
105	105	4	0.1508	9	0.067		

**Fig. 3.** Test setup: (a) front; (b) intrados (dimensions are in millimeters).

(i.e., rigid rotation of blocks was assumed). The lowest displacement rate was chosen to obtain a nominal slip rate similar to the slip rate adopted for the single-lap shear tests presented in [26]. Fig. 5a shows the average value \bar{g} of the global slips g_L and g_R measured by the transducers T4 and T5 of four specimens with textile 74/18 as a function of time. Fig. 5b shows the slip rate (obtained as the derivative of the corresponding curve of Fig. 5a) as a function of time for one specimen. Fig. 5 shows that after the initial branch the slip rate tends to be constant. Nonetheless the slip rate is significantly different from the nominal value evaluated according to the rigid blocks assumption. It can be noted that the slip rate is almost constant only at the end of the tests when the debonding has already initiated.

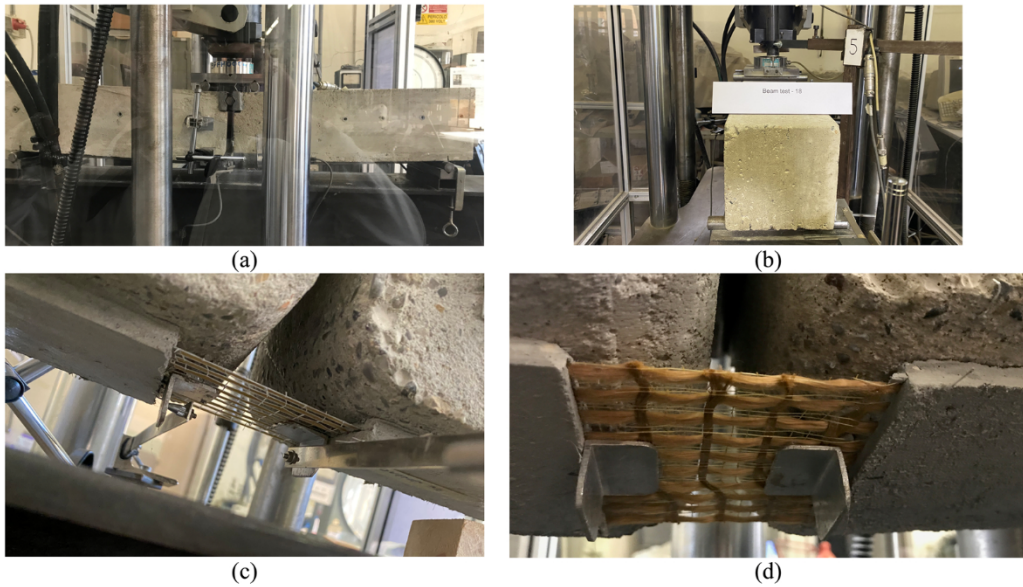
3. Experimental results and discussion

All the specimens failed due to loss of bond at the fiber-matrix interface with high interfacial slip (Fig. 4(c)–(d)). Longitudinal cracks in a plane parallel to the intrados were observed in the matrix in many of the specimens with 10 yarns of textile 70/18. Referring to textiles 105, the lack of longitudinal cracks is probably related to the absence of transverse yarns.

Fig. 6 shows a typical experimental response in terms of fiber stress-global slips g_R and g_L (transducers T4 and T5) and fiber stress-relative displacement δ of the blocks at the intrados (average of relative displacements measured by transducers T1 and T2).

Table 2Peak load F_{\max} and corresponding axial force N_{\max} , axial stress σ_{\max} , and global slip g_{\max} of the tested specimens.

Specimen	n [–]	b^* [mm]	t^* [mm]	A_f [mm ²]	F_{\max} [kN]	N_{\max} [kN]	σ_{\max} [MPa]	Average σ_{\max} [MPa]	g_{\max} [mm]	Average g_{\max} [mm]
BT_70/18_10f_0.17_01	10	4	0.1066	4.26	5.35	8.08	1895	1727 (CoV = 9%)	2.257	2.147 (CoV = 18 %)
BT_70/18_10f_0.17_02					5.19	7.84	1839		2.532	
BT_70/18_10f_0.17_03					5.08	7.66	1797		2.107	
BT_70/18_10f_0.17_04					4.78	7.22	1694		1.670	
BT_70/18_10f_0.17_05					4.12	6.21	1457		1.729	
BT_70/18_10f_0.17_06					4.75	7.17	1682		2.585	
BT_70/18_10f_0.34_01	10	4	0.1066	4.26	3.53	5.33	1250	1691 (CoV = 23%)	1.526	1.886 (CoV = 26 %)
BT_70/18_10f_0.34_02					5.29	7.98	1872		1.683	
BT_70/18_10f_0.34_03					5.51	8.32	1952		2.449	
BT_70/18_10f_0.51_01	10	4	0.1066	4.26	4.74	7.16	1680	1529 (CoV = 18 %)	1.941	1.579 (CoV = 27 %)
BT_70/18_10f_0.51_02					3.90	5.89	1382		1.615	
BT_70/18_10f_0.51_03					5.19	7.84	1839		1.763	
BT_70/18_10f_0.51_04					3.24	4.88	1145		1.700	
BT_70/18_10f_0.51_05					4.51	6.81	1598		0.859	
BT_70/18_10f_0.68_01					6.32	9.54	2238		1.994	
BT_70/18_10f_0.68_02	10	4	0.1066	4.26	7.49	11.3	2651	2243 (CoV = 16 %)	2.569	2.527 (CoV = 16 %)
BT_70/18_10f_0.68_03					7.23	10.91	2559		2.568	
BT_70/18_10f_0.68_04					5.44	8.21	1926		2.407	
BT_70/18_10f_0.68_05					5.20	7.85	1842		3.099	
BT_105_9f_0.17_01	9	4	0.15145	5.45	7.31	11.03	2023	1985 (CoV = 5 %)	3.400	3.249 (CoV = 7 %)
BT_105_9f_0.17_02					6.79	10.24	1879		3.370	
BT_105_9f_0.17_03					7.41	11.19	2053		2.976	
BT_105_9f_0.34_01	9	4	0.15145	5.45	6.62	10.00	1834	1828 (CoV = 5 %)	2.060	2.288 (CoV = 18 %)
BT_105_9f_0.34_02					6.91	10.44	1914		2.047	
BT_105_9f_0.34_03					6.27	9.46	1736		2.757	
BT_105_9f_0.51_01	9	4	0.15145	5.45	6.47	9.76	1790	1739 (CoV = 3 %)	2.881	2.657 (CoV = 11 %)
BT_105_9f_0.51_02					6.04	9.12	1672		2.781	
BT_105_9f_0.51_03					6.33	9.56	1754		2.310	
BT_105_9f_0.68_01	9	4	0.15145	5.45	9.28	14.01	2570	2516 (CoV = 2 %)	3.589	3.610 (CoV = 6 %)
BT_105_9f_0.68_02					9.03	13.63	2500		3.845	
BT_105_9f_0.68_03					8.95	13.51	2478		3.397	

**Fig. 4.** Beam tests of PBO-FRCM composites. (a) Test setup; (b) Test setup; (c) textile 105; (d) textile 70/18.

The fiber stress was computed as the ratio of the axial force N in the fibers to the area A_f of the fiber cross-section. N was computed as a function of the applied force F (Fig. 3) via equilibrium equations (Fig. 7a). The global slips measured on the two blocks g_R and g_L (points A and A', transducers T4 and T5 in Fig. 3b) were similar in the first phase of the loading process, approximately up to a load equal to 50–60 % of the joint capacity. In the second phase of the loading process the global slip increased faster at the loaded end of one of the two interface surfaces (g_R in the case shown in Fig. 6) compared to the other interface surface due to the formation and

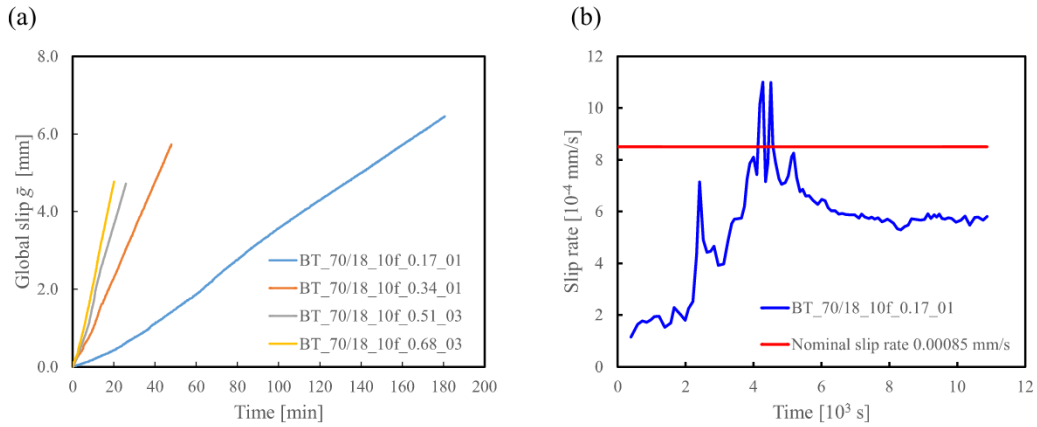


Fig. 5. (a) Global slip as a function of time; (b) slip rate as a function of time for specimen BT_70/18_10f_0.17_1.

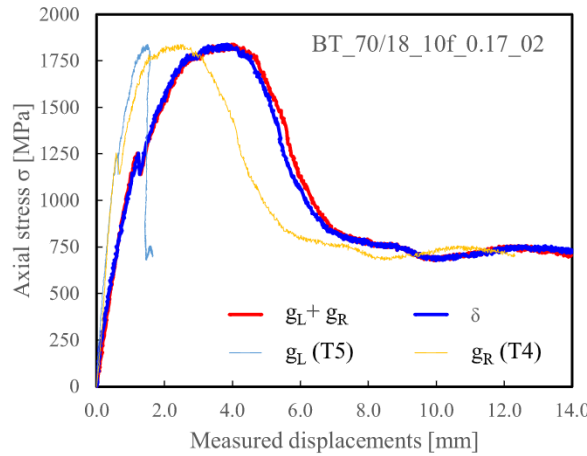


Fig. 6. Typical experimental response in terms of fiber stress-measured displacement.

propagation of a crack at the fiber-matrix interface. On this surface complete debonding occurred at the end of the test. In this phase the global slip of the other interface surface (g_L in the case shown in Fig. 6) stopped or decreased. Fig. 6 also shows that the global slips g_L and g_R are consistent with the relative displacement δ of the blocks at the intrados, since the sum of these slips equals the average relative displacement measured by the transducers T1 and T2. For each specimen, the global slip of the surface where debonding occurred is assumed as global slip g for the specimen (e.g., for specimen BT_70/18_10f_0.17_02 the global slip g is the global slip g_R , Fig. 6). The relation between the global slip and the fiber stress is named σ - g response herein.

Table 2 summarizes the specimen characteristics and the experimental results in terms of peak load F_{max} , corresponding tensile force in the fibers referred to as peak force N_{max} , corresponding stress of the fiber, referred to as peak stress σ_{max} , and global slip of the surface where debonding occurs at the peak load \bar{g}_{max} .

The average peak stress of textile 70/18 is between 1529 MPa (displacement rate 0.51 mm/min) and 2260 MPa (displacement rate 0.68 mm/min). The corresponding coefficients of variation (CoV) are equal to 18 % and 6 %, respectively. The slip at the peak load is between 1.57 mm (displacement rate 0.51 mm/min, CoV = 27 %) and 2.66 mm (rate 0.68 mm/min, CoV = 14 %). The average peak stress of textile 105 is 2516 MPa (CoV = 2 %).

The σ - g responses of the tested specimens are shown in Fig. 7. The experimental σ - g responses shown in Fig. 7 are consistent with the idealized σ - g response shown in Fig. 8a, which is associated with the typical CML shown in Fig. 8b [27] and with a bonded length equal to or longer than the effective bond length.

This typical response exhibits an ascending branch up to the debonding stress σ_{deb} , which correspond to the onset of the interfacial crack propagation that occurs for a global slip equal to s_f (Fig. 8b). A further ascending branch, up to the peak stress σ_{max} , is exhibited if a constant friction branch follows the slip s_f in the CML and the bonded length is longer than the effective bond length. The slope of this branch is related to the friction shear stress τ_f (Fig. 8b). Once the peak stress is attained, the applied stress decreases until it reaches a constant value due to friction only. The snap back phenomenon shown in Fig. 8a, which is due to the elastic energy release associated with the decrease of the force N , is not experimentally caught by the performed beam tests since they are controlled by the stroke.

An initial linear branch is exhibited by all the σ - g responses shown in Fig. 7 whose slope is related neither to the type of textile nor to

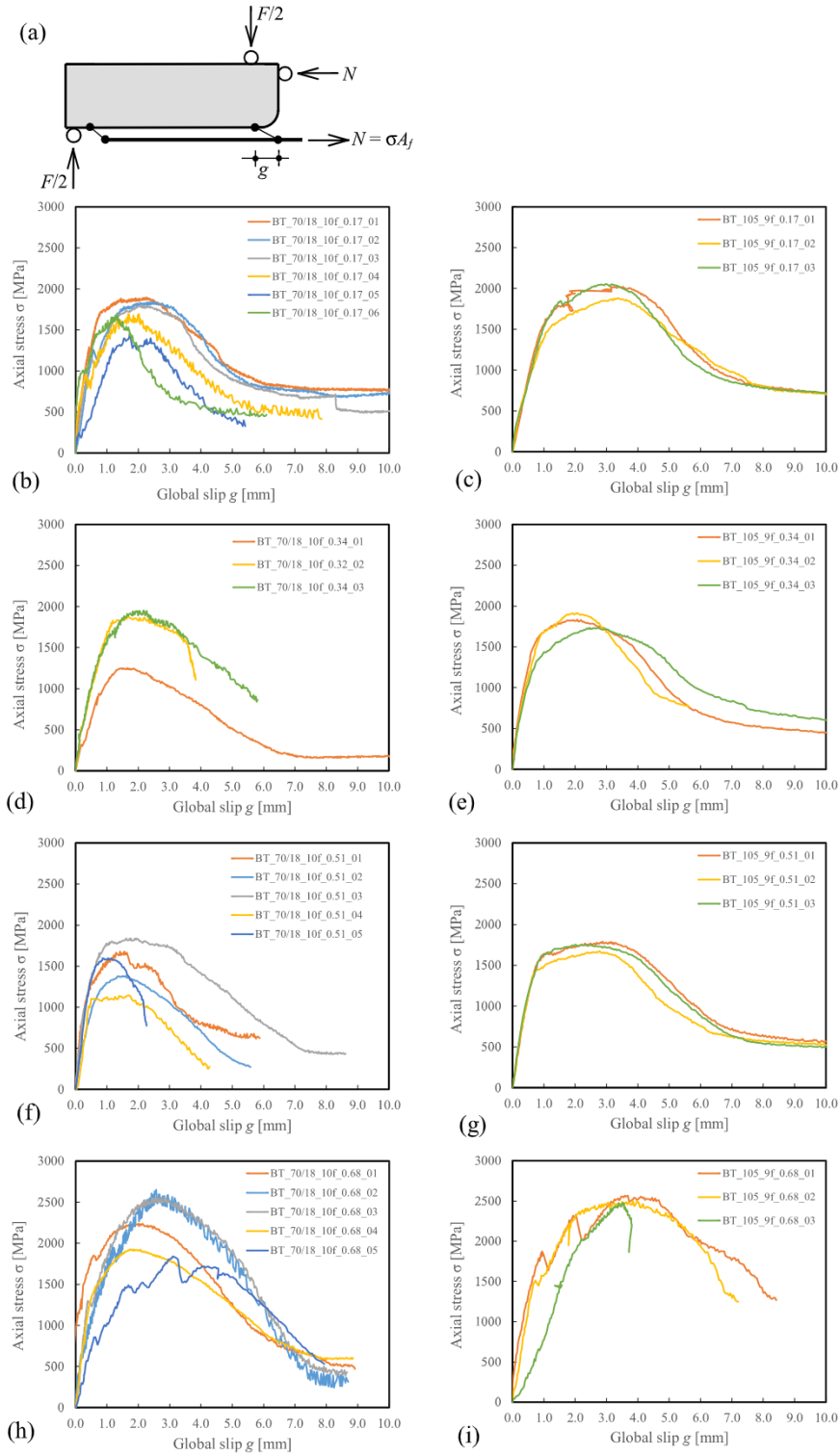


Fig. 7. (a) Beam test; (b)–(i) σ - g responses of the tested specimens.

the displacement rate. This branch is followed by an ascending branch with a smaller slope up to the onset of the debonding phenomenon. Once the debonding initiates, the increase of the load up to the peak stress σ_{max} is associated with the development of friction shear stress [277] in the debonded region near to the loaded end. The descending branch is associated with the increase of the length of the debonded zone up to the complete debonding and the attainment of a constant stress associated with the interfacial

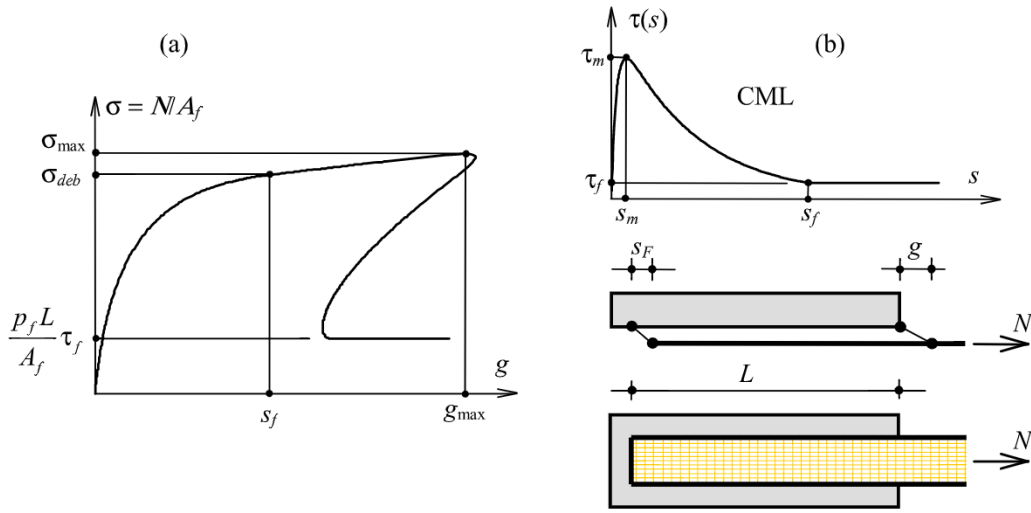


Fig. 8. (a) Idealized σ - g response; (b) typical CML.

friction shear stress τ_f [26]. It should be noted that some beam tests were stopped before reaching the friction branch to save time.

Fig. 9 compares the σ - g responses of beam test on textile 70/18, characterized by a nominal slip rate equal to 0.00085 mm/s (stroke rate equal to 0.17 mm/min), with the σ - g responses obtained by D'Antino et al. [26] on the same composite through single-lap shear tests at the slip rate of 0.00084 mm/s with a bonded length equal to 330 mm. Similar responses are obtained with the single-lap and beam tests. In particular the performed beam tests provided a slightly lower peak stress and corresponding global slip and a slightly higher friction stress compared to the values of the corresponding parameters provided by single-lap shear tests. The mentioned differences between the results of these tests are not fully consistent with the experimental results presented by Calabrese et al. [38]. In [38] it is observed that beam tests and single-lap shear tests provide similar peak stress, while beam tests provide friction stress that are roughly the double of those provided by single-lap shear test.

The higher friction stress obtained with beam tests is attributed by the authors of [38] to the transversal compressive stress on the textile at the edge of the blocks (at the mid-span of the specimen) associated with their rotation. The edges of the concrete blocks were rounded at the intrados of the hinged cross sections to reduce the transversal stress on the textile when the blocks rotate. This could explain the difference between the results presented in [38] and the results presented in this paper.

The influence of the displacement rate is shown in Fig. 10 in which the peak stress (Fig. 10a) and the corresponding global slip (Fig. 10b) are reported as a function of the nominal slip rate.

In Fig. 10 the experimental results are compared with those obtained by Carloni et al. [40] with single-lap shear tests. Experimental peak stress of single-lap shear tests presented in [40] refer to bonded length equal to 330 mm and 430 mm. It can be observed that the dependencies of the peak stress and corresponding global slip on the slip rate are different from those presented in [40], even if the peak stress corresponding to the slip rate 0.0025 mm/s is similar. The difference between the results of beam tests and the results

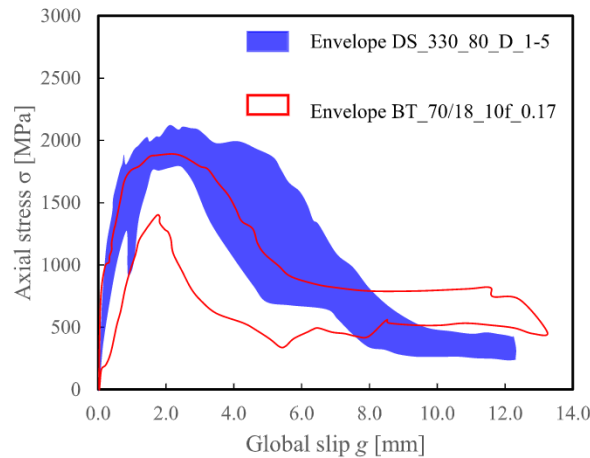


Fig. 9. Comparison between the σ - g responses obtained with beam tests and the σ - g responses obtained by D'Antino et al. [25,26] through single-lap shear tests.

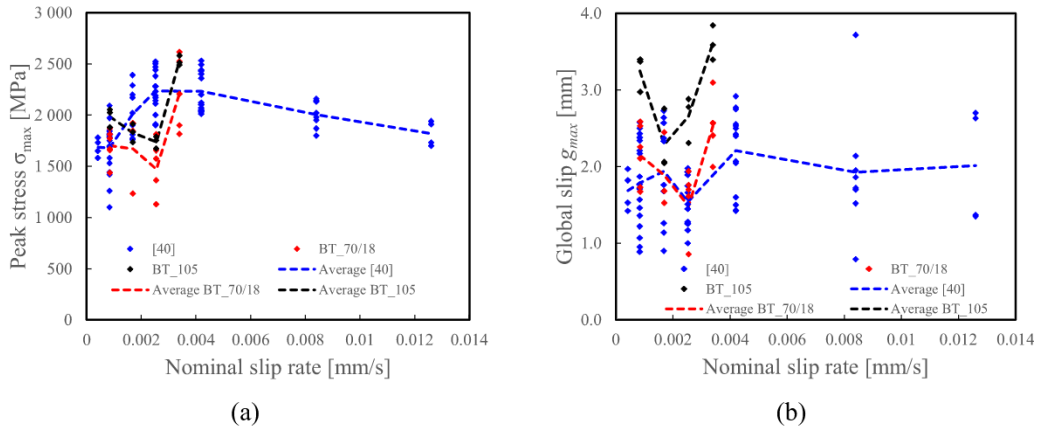


Fig. 10. Influence of the slip rate: (a) peak stress vs. slip rate; (b) global slip at peak load vs. slip rate.

reported in [40] is probably due to the different test procedure adopted. Indeed, the single-lap shear tests presented in [40] are performed imposing a constant rate of the global slip, while the beam tests are performed imposing a constant rate of the stroke. As discussed in Section 2.2 the slip rate approaches to a constant value only at an advanced stage of the test (Fig. 3). This makes the beam test configuration unsuitable for investigating the influence of the loading rate on the interfacial stress transfer phenomenon, unless the tests are controlled by the global slip measured through the transducers T4 and T5.

Fig. 11 shows the comparison among the σ - g responses of the two utilized textiles. It can be observed that the response curves of 105 are similar to those of textile 70/18. Textile 105 is characterized by slightly higher slip at peak load than those of 70/18.

3.1. Determination of the CML

The procedure proposed in [40] was applied to the presented experimental σ - g responses to obtain the parameters of a trilinear CML (Fig. 12) for the tested PBO-FRCM composites [45]. The procedure is based on the assumption that the bonded length L is long enough that the experimental σ - g response corresponding to the actual value of L is similar to the σ - g response corresponding to $L \rightarrow \infty$. The analytical σ - g response corresponding to $L \rightarrow \infty$ can be expressed as [27,41,46]

$$\sigma(g) = \sqrt{\frac{2p_f}{E_f A_f} \int_0^g \tau(s) ds} \quad (1)$$

where p_f is the matrix-fiber interface contact perimeter, and A_f and E_f are the fiber cross-sectional area and elastic modulus, respectively. The parameters of a trilinear CML with final constant friction branch (Figure) are: the peak shear stress τ_m and corresponding slip s_m , the friction shear stress τ_f , and the slip s_f at the beginning of the friction branch.

Any experimental σ - g response allows a trilinear CML to be determined. In particular:

- the friction shear stress τ_f is determined based on the final constant branch of the experimental σ - g response;
- the slope h of the ascending branch of the CML (i.e., the ratio τ_m/s_m) is determined based on the initial slope of the experimental σ - g response;
- the slip s_f is determined as the slip corresponding to the shear stress τ_f in the τ - s relation derived from the experimental σ - g response using Eq. (1);
- the fracture energy G_F is determined based on the stress σ_{deb} , evaluated as the stress corresponding to s_f in the experimental σ - g response;
- the slip s_m and the shear stress τ_m are finally determined as

$$s_m = \frac{2G_F - \tau_f s_f}{h s_f - \tau_f} \quad (2)$$

$$\tau_m = h s_m \quad (3)$$

The procedure was applied to the σ - g responses of the specimen tested up to the final friction branch at a displacement rate of 0.17 mm/min (nominal slip rate equal to 0.00085 mm/s). Fig. 13 summarizes the obtained CMLs for the 70/18 (Fig. 13a) and 105 (Fig. 13b) textiles. Fig. 13 also shows the average trilinear CMLs for the tested PBO-FRCM composites. The average trilinear CMLs were obtained by best fitting (least square method was employed) with a trilinear CML the $\tau(s)$ curve obtained by averaging the ordinates of the CML of single specimens.

In Fig. 14, the obtained average CML of the PBO-FRCM composite with the 70/18 textile is compared with the CML obtained for the same PBO-FRCM composite by Focacci et al. [27] from the results of single-lap shear tests using an indirect calibration method based on the joint capacity response and the CML obtained for the same PBO-FRCM composite by D'Antino et al. [26] using a direct

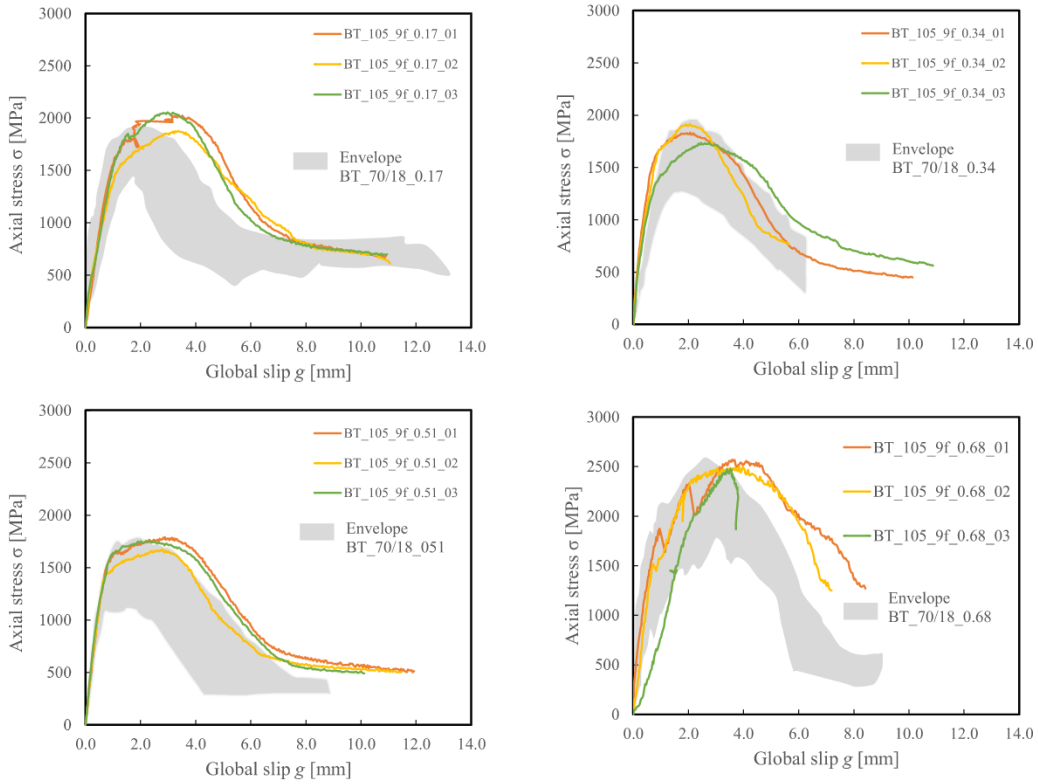


Fig. 11. Effect of the fiber arrangement on the σ - g responses to textile 105 vs. textile 70/18.

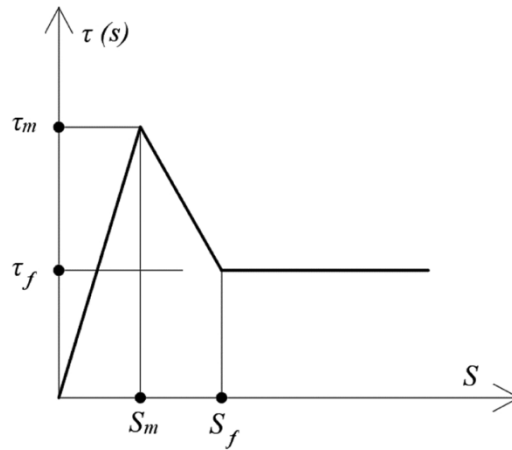


Fig. 12. Trilinear CML with friction constant branch.

calibration method based on the profile of the strain along the bonded length.

Fig. 14 shows that in relation to the PBO-FRCM with the 70/18 textile the simple procedure proposed in [41] applied to the σ - g responses obtained from the beam tests allows to define a CML relationship similar to the one obtained applying the more complex procedure described in [27] relative to the results of the single-lap shear test. It should be noticed that the application of the procedure described in [27] requires the execution of tests with different bond lengths. In particular the fracture energy associated with the CML relationship obtained from the results of the beam tests for the PBO-FRCM with the 70/18 textile is 0.20 N/mm and is similar to the fracture energy associated to the law obtained with the procedure described in [27], which is equal to 0.19 N/mm.

The procedure based on the deformation profile [26] is instead characterized by higher shear stresses. This is probably due to the fact that in the procedure used in [26] the deformation measured on the surface of the yarns is used, which is higher than the average deformation of the fibers, while in the procedures proposed in [41] and in [27] the average deformation of the fiber obtained starting

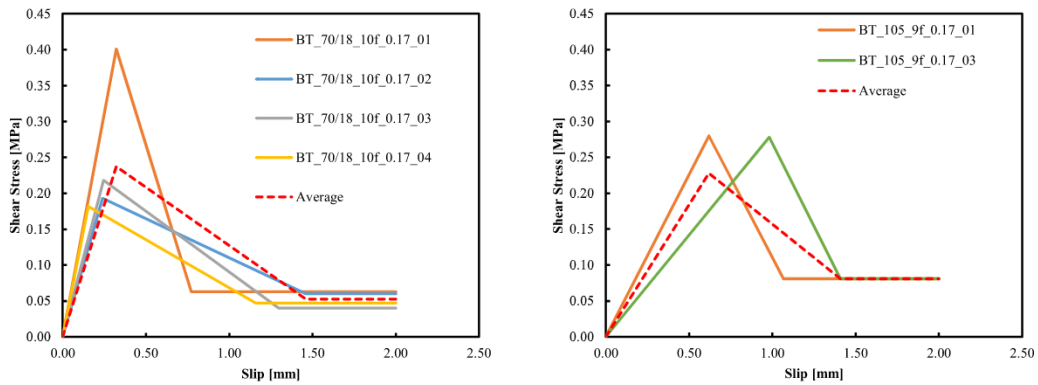


Fig. 13. CMLs obtained with the procedure proposed in [40] based on σ -g responses of the specimen tested at a displacement rate of 0.17 mm/min and average CMLs. (a) PBO-FRCM with textile 70/18. (b) PBO-FRCM with textile 105.

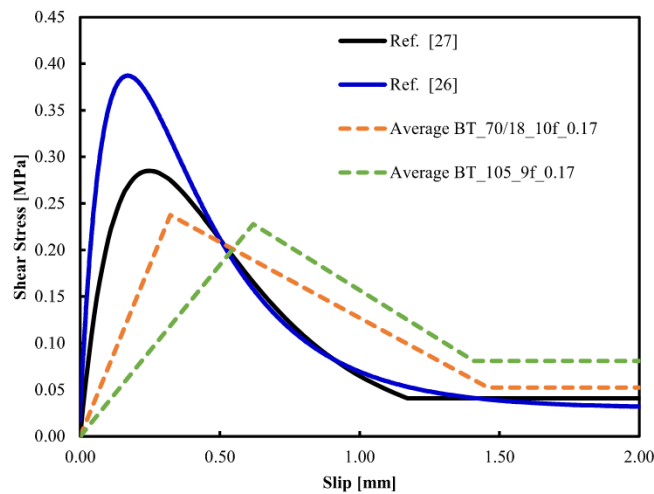


Fig. 14. Comparison of the average CMLs obtained based on the results of beam tests with the CMLs of the PBO-FRCM with textile 70/18 obtained by Focacci et al. [27] and by D'Antino et al. [26] from the results of single-lap shear tests.

from the tensile strength of the fibers themselves is used.

4. Conclusions

This paper presents the results of the first step of an experimental campaign for the characterization of the bond between PBO-FRCM materials and concrete by means of beam tests. Two composite materials made of the same matrix and different PBO textiles were tested. The tests were performed with different loading rates. The following conclusions can be drawn.

1. Beam tests provided experimental responses similar to those obtained by several authors through single-lap shear tests.
2. The fiber stress associated with the friction at the fiber-matrix interface was lower than that obtained by other authors with similar tests. This difference can be ascribed to the geometrical characteristics of the employed specimen.
3. It was not possible to observe a clear dependence of the joint capacity and the corresponding global slip on the loading rate. Therefore beam test does not appear suitable for evaluating the effect of the loading rate on the bond properties of PBO-FRCM materials, unless they are performed controlling the relative displacement between the concrete blocks or the interfacial slip at the mid-span of the specimen.
4. Textiles of PBO fibers with different fiber amounts have comparable responses in terms of shear stress transfer mechanism in the investigated range.
5. The cohesive material law that can be obtained from the results of beam tests is similar to that obtained with the results of single-lap shear tests.

The beam test appears to be an alternative to single-lap or double-lap shear tests to characterize the interface between FRCM

materials and the substrate. However further investigations are needed to determine the influence of the geometry of the specimen and the test procedure on the measured parameters.

Declaration of Competing Interest

The authors declare that they have no known competing financial interests or personal relationships that could have appeared to influence the work reported in this paper.

Data Availability

Data will be made available on request.

Acknowledgments

The authors greatly acknowledge Ruregold s.r.l. (Italy) for providing the composite materials used in this experimental work.

References

- [1] DT 200, Italian National Research Council (CNR), Guide for the Design and Construction of Externally Bonded FRP Systems for Strengthening Existing Structures, CNR - Rome, Italy, 2004.
- [2] ACI Committee 440.1R-15, Guide for the Design and Construction of Structural Concrete Reinforced with Fiber-Reinforced Polymer (FRP) Bars, ACI 440.1R-15, Farmington Hill, US, 2015.
- [3] DT 215, Italian National Research Council (CNR), Guide for the Design and Construction of Externally Bonded Fibre Reinforced Inorganic Matrix Systems for Strengthening Existing Structures, CNR - Rome, Italy, 2020.
- [4] ACI Committee 549, Guide to Design and Construction of Externally Bonded Fabric-reinforced Cementitious Matrix (FRCM) Systems for Repair and Strengthening Concrete and Masonry Structures, ACI 549.4R-13, Farmington Hill, US, 2013.
- [5] G. Loreto, L. Leardini, D. Arboleda, A. Nanni, Performance of RC slab-type elements strengthened with fabric-reinforced cementitious-matrix composites, *J. Compos. Constr.* 18 (3) (2014), [https://doi.org/10.1061/\(ASCE\)CC.1943-5614.0000415](https://doi.org/10.1061/(ASCE)CC.1943-5614.0000415).
- [6] S. Babaeidarabad, G. Loreto, A. Nanni, Flexural strengthening of RC beams with an externally bonded fabric-reinforced cementitious matrix, *J. Compos. Constr.* 18 (5) (2014) 04014009, [https://doi.org/10.1061/\(ASCE\)CC.1943-5614.0000473](https://doi.org/10.1061/(ASCE)CC.1943-5614.0000473).
- [7] C. Escrig, L. Gil, E. Bernat-Maso, Experimental comparison of reinforced concrete beams strengthened against bending with different types of cementitious-matrix composite materials, *Constr. Build. Mater.* 137 (2017) 317–329, <https://doi.org/10.1016/j.conbuildmat.2017.01.106>.
- [8] F. Bencardino, C. Carloni, A. Cordello, F. Focacci, A. Napoli, R. Realfonzo, Flexural behaviour of RC members strengthened with FRCM: state-of-the-art and predictive formulas, *Compos. Part B: Eng.* 148 (2018) 132–148.
- [9] L. Ombres, Structural performances of reinforced concrete beams strengthened in shear with a cement based fiber composite material, *Compos. Struct.* 122 (2015) 316–329, <https://doi.org/10.1016/j.compstruct.2014.11.059>.
- [10] A. D'Ambrisi, F. Focacci, Flexural strengthening of RC beams with cement-based composites, *J. Compos. Constr.* 15 (5) (2011) 707–720, [https://doi.org/10.1061/\(ASCE\)CC.1943-5614.0000218](https://doi.org/10.1061/(ASCE)CC.1943-5614.0000218).
- [11] Z.C. Tetta, L.N. Koutas, D.A. Bournas, Textile-reinforced mortar (TRM) versus fiber-reinforced polymers (FRP) in shear strengthening of concrete beams, *Compos. Part B: Eng.* 77 (2015) 338–348, <https://doi.org/10.1016/j.compositesb.2015.03.055>.
- [12] Zoi C. Tetta, Thanasis C. Triantafyllou, Dionysios A. Bournas, On the design of shear-strengthened RC members through the use of textile reinforced mortar overlays, *Compos. Part B: Eng.* 147 (2018) 178–196.
- [13] T. D'Antino, F. Focacci, L.H. Sneed, C. Carloni, Relationship between the effective strain of PBO FRCM-strengthened RC beams and the debonding strain of direct shear tests, *Eng. Struct.* 216 (2020), 110631, <https://doi.org/10.1016/j.engstruct.2020.110631>.
- [14] Consiglio Superiore dei Lavori Pubblici - Servizio Tecnico Centrale, Linea Guida per la identificazione, la qualificazione ed il controllo di accettazione di compositi fibrorinforzati a matrice inorganica (FRCM) da utilizzarsi per il consolidamento strutturale di costruzioni esistenti, Consiglio Superiore dei Lavori Pubblici - Servizio Tecnico Centrale, Dec. 2018.
- [15] AC 434-13, Acceptance criteria for masonry and concrete strengthening using fabric-reinforced cementitious matrix (FRCM) composite systems, 2013.
- [16] C. Carloni, K.V. Subramaniam, FRP-masonry debonding: numerical and experimental study of the role of mortar joints, *J. Compos. Constr.* 16 (5) (2012) 581–589, [https://doi.org/10.1061/\(ASCE\)CC.1943-5614.0000282](https://doi.org/10.1061/(ASCE)CC.1943-5614.0000282).
- [17] M. Malena, F. Focacci, C. Carloni, G. de Felice, The effect of the shape of the cohesive material law on the stress transfer at the FRP-masonry interface, *Compos. Part B: Eng.* 110 (2017) 368–380, <https://doi.org/10.1016/j.compositesb.2016.11.012>.
- [18] M. Bocciarelli, M.A. Pisani, Survey on the interface behaviour in reinforced concrete beams strengthened with externally bonded FRP reinforcement, *Compos. Part B: Eng.* 118 (2017) 169–176, <https://doi.org/10.1016/j.compositesb.2017.02.047>.
- [19] C. Carloni, et al., Fiber reinforced composites with cementitious (inorganic) matrix, in: C. Pellegrino, J. Sena-Cruz (Eds.), *Design Procedures for the Use of Composites in Strengthening of Reinforced Concrete Structures*, 19, Springer Netherlands, Dordrecht, 2016, pp. 349–392.
- [20] A. Cascardi, R. Dell'Anna, F. Micelli, F. Lionetto, M.A. Aiello, A. Maffezzoli, Reversible techniques for FRP-confinement of masonry columns, *Constr. Build. Mater.* 225 (2019) 415–428.
- [21] L. Ombres, Analysis of the bond between Fabric Reinforced Cementitious Mortar (FRCM) strengthening systems and concrete, *Compos. Part B: Eng.* 69 (2015) 418–426, <https://doi.org/10.1016/j.compositesb.2014.10.027>.
- [22] L. Ascione, G. de Felice, S. De Santis, A qualification method for externally bonded Fibre Reinforced Cementitious Matrix (FRCM) strengthening systems, *Compos. Part B: Eng.* 78 (2015) 497–506, <https://doi.org/10.1016/j.compositesb.2015.03.079>.
- [23] L.H. Sneed, T. D'Antino, C. Carloni, C. Pellegrino, A comparison of the bond behavior of PBO-FRCM composites determined by double-lap and single-lap shear tests, *Cem. Concr. Compos.* 64 (2015) 37–48, <https://doi.org/10.1016/j.cemconcomp.2015.07.007>.
- [24] F.G. Carozzi, et al., Experimental investigation of tensile and bond properties of carbon-FRCM composites for strengthening masonry elements, *Compos. Part B: Eng.* 128 (2017) 100–119, <https://doi.org/10.1016/j.compositesb.2017.06.018>.
- [25] C. Caggegi, et al., Experimental analysis on tensile and bond properties of PBO and aramid fabric reinforced cementitious matrix for strengthening masonry structures, *Compos. Part B: Eng.* 127 (2017) 175–195, <https://doi.org/10.1016/j.compositesb.2017.05.048>.
- [26] T. D'Antino, C. Carloni, L.H. Sneed, C. Pellegrino, Matrix-fiber bond behavior in PBO FRCM composites: a fracture mechanics approach, *Eng. Fract. Mech.* 117 (2014) 94–111, <https://doi.org/10.1016/j.engfracmech.2014.01.011>.
- [27] F. Focacci, T. D'Antino, C. Carloni, L.H. Sneed, C. Pellegrino, An indirect method to calibrate the interfacial cohesive material law for FRCM-concrete joints, *Mater. Des.* 128 (2017) 206–217, <https://doi.org/10.1016/j.matdes.2017.04.038>.
- [28] A. D'Ambrisi, L. Feo, F. Focacci, Experimental analysis on bond between PBO-FRCM strengthening materials and concrete, *Compos. Part B: Eng.* 44 (1) (2013) 524–532, <https://doi.org/10.1016/j.compositesb.2012.03.011>.

- [29] M.R. Valluzzi, et al., Round Robin Test for composite-to-brick shear bond characterization, *Mater. Struct.* 45 (12) (2012) 1761–1791, <https://doi.org/10.1617/s11527-012-9883-5>.
- [30] S. De Santis, et al., Round Robin Test on tensile and bond behaviour of steel reinforced grout systems, *Compos. Part B: Eng.* 127 (2017) 100–120, <https://doi.org/10.1016/j.compositesb.2017.03.052>.
- [31] A. D'Ambrosi, L. Feo, F. Focacci, Bond-slip relations for PBO-FRCM materials externally bonded to concrete, *Compos. Part B: Eng.* 43 (8) (2012) 2938–2949, <https://doi.org/10.1016/j.compositesb.2012.06.002>.
- [32] F. Focacci, T. D'Antino, C. Carloni, The role of the fiber–matrix interfacial properties on the tensile behavior of FRCM coupons, *Constr. Build. Mater.* 265 (2020), 120263, <https://doi.org/10.1016/j.conbuildmat.2020.120263>.
- [33] F. Focacci, T. D'Antino, C. Carloni, Tensile testing of FRCM coupons for material characterization: discussion of critical aspects, *J. Compos. Constr.* (2022), [https://doi.org/10.1061/\(ASCE\)CC.1943-5614.0001223](https://doi.org/10.1061/(ASCE)CC.1943-5614.0001223) (in press).
- [34] E. Fazzi, G. Misseri, L. Rovero, G. Stipo, Finite difference model for the bond behaviour of polyparaphenylene benzobi-soxazole (PBO) fibre-reinforced composite system for retrofitting masonry, *Key Eng. Mater.* 916 (2022) 425–432, <https://doi.org/10.4028/p-6848f4>.
- [35] E. Grande, G. Milani, M. Imbimbo, Theoretical model for the study of the tensile behavior of FRCM reinforcements, *Constr. Build. Mater.* 236 (2019), 117617, <https://doi.org/10.1016/j.conbuildmat.2019.117617>.
- [36] P. Colombi, T. D'Antino, Analytical assessment of the stress-transfer mechanism in FRCM composites, *Compos. Struct.* 220 (2019) 961–970, <https://doi.org/10.1016/j.compstruct.2019.03.074>.
- [37] A.S. Calabrese, P. Colombi, T. D'Antino, A bending test set-up for the investigation of the bond properties of FRCM strengthenings applied to masonry substrates, *KEM 817* (2019) 149–157, <https://doi.org/10.4028/www.scientific.net/KEM.817.149>.
- [38] A.S. Calabrese, T. D'Antino, P. Colombi, C. Poggi, Study of the influence of interface normal stresses on the bond behavior of FRCM composites using direct shear and modified beam tests, *Constr. Build. Mater.* 262 (2020), 120029, <https://doi.org/10.1016/j.conbuildmat.2020.120029>.
- [39] A.S. Calabrese, T. D'Antino, P. Colombi, Experimental and analytical investigation of PBO FRCM-concrete bond behavior using direct and indirect shear test set-ups, *Compos. Struct.* 267 (2021), 113672, <https://doi.org/10.1016/j.compstruct.2021.113672>.
- [40] C. Carloni, S. Verre, L.H. Sneed, L. Ombres, Loading rate effect on the debonding phenomenon in fiber reinforced cementitious matrix-concrete joints, *Compos. Part B: Eng.* 108 (2017) 301–314, <https://doi.org/10.1016/j.compositesb.2016.09.087>.
- [41] F. Focacci, T. D'Antino, C. Carloni, Determination of the matrix-fiber cohesive material law of FRCM-concrete joints, *Key Eng. Mater.* 919 (2022) 55–56, <https://doi.org/10.4028/p-366hdm>.
- [42] EN 1015-11:2019, Methods of Test for Mortar for Masonry – Part 11: Determination of Flexural and Compressive Strength of Hardened Mortar, UNI EN, 2019.
- [43] (<https://www.bigmat.it/prodotti-a-marchio/edilizia/dettaglio/calcestruzzo-bigmat>).
- [44] EN 12390-3:2019, Testing Hardened Concrete – Part 3: Compressive Strength of Test Specimens, UNI EN, 2019.
- [45] V. Bertolli, T. D'Antino, Modeling the behavior of externally bonded reinforcement using a rigid-trilinear cohesive material law, *Int. J. Solids Struct.* 248 (2022), <https://doi.org/10.1016/j.ijsolstr.2022.111641>.
- [46] A.S. Calabrese, P. Colombi, T. D'Antino, Analytical solution of the bond behavior of FRCM composites using a rigid-softening cohesive material law, *Compos. Part B: Eng.* 174 (2019), <https://doi.org/10.1016/j.compositesb.2019.107051>.